Available online at www.sciencedirect.com
ScienceDirect
Catalysis Today 129 (2007) 110–117
CATALYSIS TODAY
www.elsevier.com/locate/cattod

Scaling-up of slurry reactors for the photocatalytic degradation of 4-chlorophenol

María L. Satuf, Rodolfo J. Brandi, Alberto E. Cassano, Orlando M. Alfano *

INTEC-Universidad Nacional del Litoral and CONICET, Güemes 3450, S3000GLM, Santa Fe, Argentina

Available online 8 August 2007

Abstract

A kinetic expression to represent the photocatalytic degradation of 4-chlorophenol (4-CP) has been derived in a small, well-stirred, slurry reactor. Based on a plausible reaction sequence, the obtained mathematical representation describes with good accuracy the decomposition of 4-CP as well as the evolution of the most important reaction intermediates. This information is used to actionate a very different reactor in size, shape and operating conditions. The adopted approach consists in the precise modeling of the laboratory reactor to estimate intrinsic kinetic parameters. Afterward, the reaction kinetics obtained in the small reactor is used to model a bench scale reactor, without employing any adjustable parameters. Simulation results are in good agreement with the experimental data obtained in the larger reactor. This approach points to the development of a full scale-up procedure employing exclusively laboratory reactor information.

Keywords: Photocatalysis; Scaling-up; Slurry reactors; 4-Chlorophenol; Degradation

1. Introduction

Photocatalysis employing titanium dioxide (TiO_2) has proven to be a useful method to remove a wide variety of organic and inorganic pollutants from water and air [1–3]. Although considerable research on the chemistry of the process has been made, no parallel effort in the engineering aspects of photocatalysis has been reported [4].

Reactor modeling is essential for the application of heterogeneous photocatalysis on an industrial scale [5]. The traditional, purely empirical methodology for scaling-up starts from laboratory experiments and gradually increases the size of the proposed reactor up to the desired commercial size device. This approach is simple but requires significant investments. Scaling-up procedures employing mathematical models based on the fundamentals of chemical engineering can reduce expensive and time-consuming steps.

The literature reports different approaches involving the modeling of photoreactors for water treatment. Giménez et al. [6] presented the modeling of the reaction kinetics of phenol and 2,4-dichlorophenol in two different pilot size solar reactors: compound parabolic collector (CPC) modules and a flat reactor. The approach consists of the combination of fundamental principles together with adjustable constants that depend directly on the type of reactor under analysis and, mainly, on the reactor shape and configuration. Results indicate that further studies are needed, particularly to apply the kinetic model to larger size devices or different geometries. Another approach, based on fundamental principles, was applied to perform a scale-up of a homogeneous photoreactor [7]. They moved directly from laboratory experiments in a very small, well-mixed reactor (reactor volume = 70 cm^3) to a large scale, continuous flow, annular reactor of 2 m long without employing any adjustable parameters. Reasonably good results were achieved. Thereafter, Li Puma et al. [5,8,9] presented the mathematical modeling of different types of slurry photocatalytic reactors using solar and artificial light. The models could be applied for scaling-up purposes, but not specific attempts were made in this direction. Zhang et al. [10,11] proposed a different approach to model fixed-film photocatalytic reactors. Results from a flat plate reactor, illuminated with UV lamps, were used to fit a semi-empirical kinetic model for the degradation of 4-CP. This model was then employed to predict the performance of a corrugated plate solar reactor. Theoretical predictions were found to agree

* Corresponding author. Tel.: +54 342 451 1546; fax: +54 342 451 1087.
E-mail address: alfano@intec.unl.edu.ar (O.M. Alfano).

0920-5861/$ – see front matter © 2007 Elsevier B.V. All rights reserved.
doi:10.1016/j.cattod.2007.06.056

well with the experimental data, but no significant changes in size were observed in both apparatus. Finally, the determination of intrinsic kinetic constants to scale-up the photo-Fenton process was presented by Rodríguez et al. [12]. The initial mineralization rate constant for phenol was evaluated in a laboratory scale reactor (solar simulator) and in a pilot scale CPC reactor, assuming a first order reaction. The kinetic constants calculated for both reactors were very similar, thus concluding that they are independent of the radiation source and the geometry of the reactor.

In the present work, we develop a methodology to achieve the scale-up of a photocatalytic reaction directly from laboratory data to a reactor of larger size, different configuration and mode of operation. The degradation of 4-chlorophenol (4-CP) was the reaction employed to validate the scaling-up proposal.

The photomineralization of 4-CP has been the subject of numerous studies, particularly because it has been considered as one of the potential candidates to become a model compound for reporting comparative photocatalytic efficiency results. Research publications concerning the degradation of 4-CP include information about the reaction intermediates and the possible degradation pathways under different experimental conditions [13–15]. Based on these reports, a kinetic model for the degradation of 4-CP was derived. The model describes the evolution of 4-CP as well as the formation and disappearance of the main intermediate products: 4-chlorocatechol (4-CC) and hydroquinone (HQ). The results obtained in a laboratory scale slurry reactor were applied to predict the performance of a reactor of different geometry, size, irradiation rate and operating conditions.

2. Proposed methodology

The proposed methodology for scaling-up photocatalytic slurry reactors is summarized in Fig. 1. It consists of two principal parts. The first one involves the derivation of an intrinsic kinetic expression, i.e., independent of the actual values of the reactor configuration, radiation source and experimental conditions, to represent the photocatalytic degradation of the model compound (4-CP) in a laboratory scale reactor. The kinetic expression is based on a detailed reaction scheme and incorporates the effects of irradiation rates, pollutant concentration, and catalyst loading.

A precise evaluation of the radiation field inside the reactor is required to model the effect of radiation absorption on the reaction rate. The complexity of radiation modeling in heterogeneous systems lies in the simultaneous existence of absorption and scattering. The application of the radiative transfer equation (RTE) represents a rigorous way of determining the spatial and directional distribution of photon absorption in slurry reactors.

The mass balances of the pollutant and, according to the particular reaction, the intermediate products, are solved in order to obtain the theoretical evolution of the species involved. The mass balances include the information of the kinetic and radiation models. The estimation of the kinetic parameters is achieved by applying a nonlinear optimization program to adjust the model predictions to the experimental data. Experimental conditions must ensure that the reaction is under kinetic control to avoid the effect of mass transfer limitations.

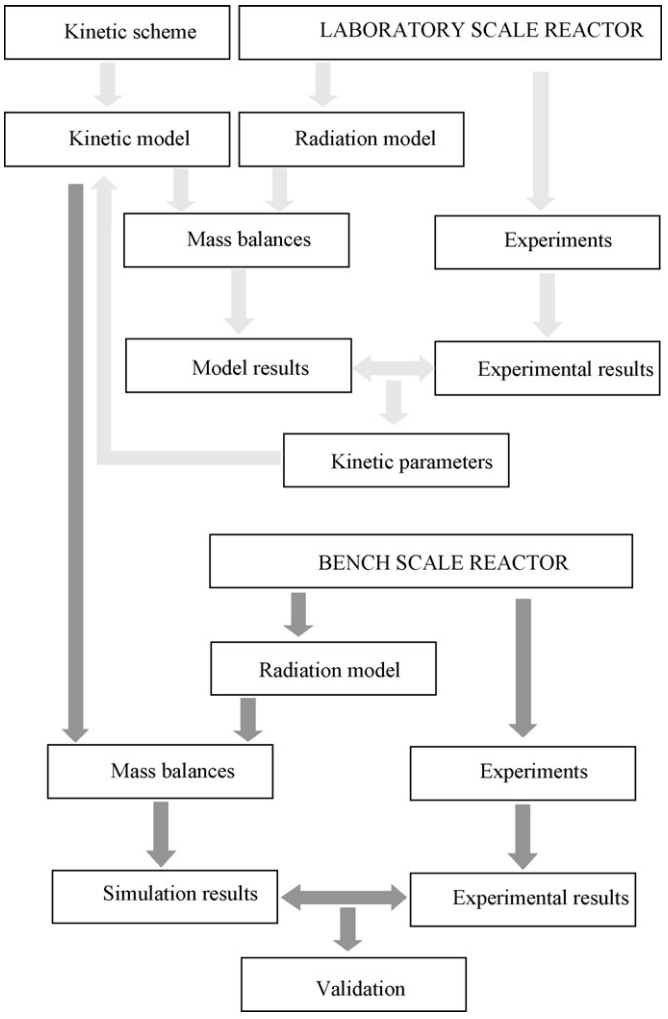

Fig. 1. Flow chart of the employed scaling-up methodology.

The second part of the scaling-up procedure involves the application of the kinetic model on a bench scale reactor. The radiation model and mass balances are solved in the new reactor, and the kinetic expressions developed in the laboratory reactor are directly incorporated in the mass balances. Data obtained from experimental runs in the bench scale reactor are then compared with simulation results in order to validate the procedure.

3. Modeling of the laboratory scale reactor

3.1. Reactor description and set-up

The kinetic study was carried out in a cylindrical reactor made of stainless steel and Teflon, with two circular borosilicate glass windows. It operates as a slurry reactor inside the loop of a batch recycle system. The reactor has a special mechanism of mobile windows that allows one to modify the length L_R (Fig. 2).

Radiation was supplied by two sets of four UV, tubular lamps (UV Phillips TL 4W/08), placed at both sides of the

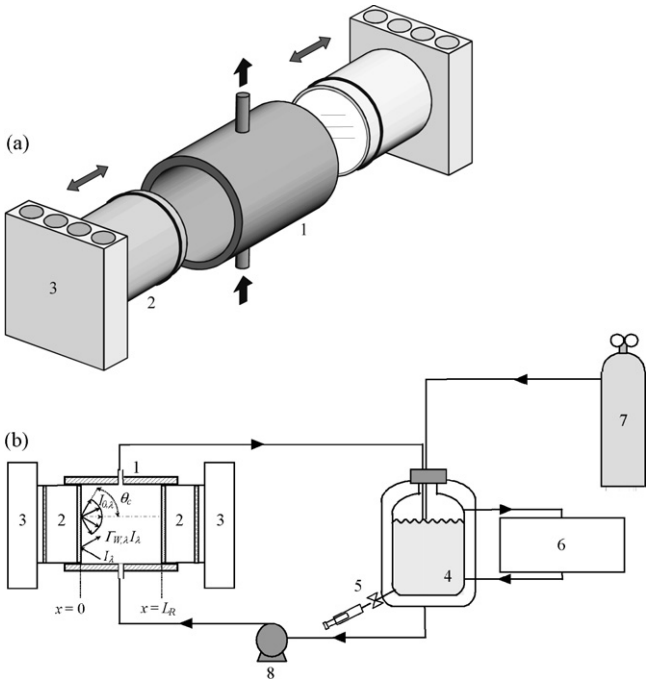

Fig. 2. Schematic representation of the laboratory scale experimental device. (a) View of the reactor. (b) Setup. Keys: (1) reactor; (2) mobile windows system; (3) radiation emitting system; (4) tank; (5) sampling valve; (6) thermostatic bath; (7) oxygen supply; (8) pump.

reactor. Optical filters were interposed between the lamps and the reactor to modify the level of incident radiation. Ground glass plates, situated between the lamps and the reactor windows, were used to produce diffuse inlet radiation. The storage tank was equipped with a sampling valve, a gas inlet for oxygen supply, and a water-circulating jacket to ensure isothermal conditions during the reaction time (Fig. 2b). The system was maintained under overpressure of oxygen to guarantee the renewal of the oxygen consumed by the photochemical reaction. The pump flow rate was adjusted in order to provide good mixing conditions, low conversion per pass in the reactor, and uniform concentration of the catalyst throughout the system. The dimensions and main characteristics of the laboratory scale reactor are summarized in Table 1.

Table 1
Dimensions and emitting system characteristics of the laboratory and bench scale reactors

Description	Laboratory scale reactor	Bench scale reactor
Main dimensions	Inner diameter = 8.6 cm Length = 0.5–5.0 cm	Width = 18.0 cm Length = 34.0 cm Thickness = 1.2 cm
Reactor volume	29.0–290.4 cm^3	734.4 cm^3
Total system volume	1000 cm^3	5000 cm^3
No. of lamps	8	2
Nominal input power	4 W (per lamp)	40 W (per lamp)
Emission range	300–400 nm	310–410 nm
Radiation flux (100%)	7.55×10^{-9} Einstein cm^{-2} s^{-1}	6.40×10^{-9} Einstein cm^{-2} s^{-1}
Lamp diameter	1.6 cm	3.8 cm
Lamp arc length	13.6 cm	60 cm

3.2. Mass balances

Considering that (i) there is a differential conversion per pass in the reactor, (ii) the system is perfectly stirred, (iii) there are no mass transport limitations, (iv) the chemical reaction occurs only at the solid–liquid interface [16,17], and (v) direct photolysis is neglected [18], the mass balance for the species i in the system takes the following form [19]:

$$\varepsilon_L \left.\frac{dC_i(t)}{dt}\right|_{Tk} = \frac{V_R}{V_T} a_v \langle \nu_i r(\mathbf{x},t)\rangle_{A_R}, \quad i = \text{4-CP, 4-CC, HQ} \quad (1)$$

where ε_L is the liquid hold-up ($\varepsilon_L \cong 1$), C_i the molar concentration of i (mol cm^{-3}), t denotes reaction time, Tk refers to the tank, V_R the reactor volume (cm^3), V_T the total system volume (cm^3), a_v denotes the catalytic surface area per unit suspension volume (cm^{-1}), ν_i the stoichiometric coefficient, and $\langle r(\mathbf{x},t)\rangle_{A_R}$ is the superficial reaction rate averaged over the catalytic reaction area (mol cm^{-2} s^{-1}).

The primary oxidation products of 4-CP are 4-chlorocatechol (4-CC), hydroquinone (HQ), and benzoquinone (BQ) [14]. Under the experimental conditions employed in our work, at pH 2.5, the oxidation via 4-CC represents the main pathway for the degradation of 4-CP. In second place appears the formation of HQ. Because of the low concentrations of BQ found during the experiments, this intermediate product is not considered in the kinetic model. Then, the mass balances for 4-CP, 4-CC and HQ, with the corresponding initial conditions are

$$\varepsilon_L \frac{dC_{\text{4-CP}}(t)}{dt} = -\frac{V_R}{V_T} a_v \{\langle r_{\text{4-CP,1}}(\mathbf{x},t)\rangle_{A_R} + \langle r_{\text{4-CP,2}}(\mathbf{x},t)\rangle_{A_R}\},$$
$$C_{\text{4-CP}}(t=0) = C_{\text{4-CP,0}} \quad (2)$$

$$\varepsilon_L \frac{dC_{\text{4-CC}}(t)}{dt} = \frac{V_R}{V_T} a_v \{\langle r_{\text{4-CP,1}}(\mathbf{x},t)\rangle_{A_R} - \langle r_{\text{4-CC}}(\mathbf{x},t)\rangle_{A_R}\},$$
$$C_{\text{4-CC}}(t=0) = 0 \quad (3)$$

$$\varepsilon_L \frac{dC_{\text{HQ}}(t)}{dt} = \frac{V_R}{V_T} a_v \{\langle r_{\text{4-CP,2}}(\mathbf{x},t)\rangle_{A_R} - \langle r_{\text{HQ}}(\mathbf{x},t)\rangle_{A_R}\},$$
$$C_{\text{HQ}}(t=0) = 0 \quad (4)$$

Two parallel reaction pathways are postulated for the degradation of 4-CP: $r_{\text{4-CP,1}}$ represents the degradation rate to give 4-CC, whereas $r_{\text{4-CP,2}}$ is the rate that leads to the formation of HQ. $r_{\text{4-CC}}$ and r_{HQ} denote the degradation rates of 4-CC and HQ, respectively.

3.3. Kinetic model

The kinetic model proposed for the photocatalytic degradation of 4-CP is based on the reaction sequence summarized in Table 2 [20,21]. The reaction starts with the activation of TiO_2 particles with UV radiation. When the catalyst is irradiated with photons whose energy is equal to or greater than its band-gap energy, an electron from the valence band of the catalyst particle is promoted to its conduction band, leaving a positively charged hole in the valence band. The photogenerated electron–hole pair migrates to the surface of the catalyst particle and

Table 2
Kinetic steps for the 4-CP photocatalytic degradation

Step	Reaction
Activation	$TiO_2 + h\nu \rightarrow TiO_2 + e^- + h^+$
Recombination	$e^- + h^+ \rightarrow$ heat
Electron trapping	$e^- + O_{2,ads} \rightarrow {}^{\bullet}O_2^-$
Hole trapping	$h^+ + H_2O_{ads} \rightarrow {}^{\bullet}OH + H^+$
	$h^+ + OH_{ads}^- \rightarrow {}^{\bullet}OH$
Hydroxyl attack	$4\text{-}CP_{ads} + {}^{\bullet}OH \rightarrow \rightarrow X_i$
	$X_{i,ads} + {}^{\bullet}OH \rightarrow X_j$
	$Y_{i,ads} + {}^{\bullet}OH \rightarrow Y_j$

reacts with surface species. The electrons and holes have to be trapped to prevent recombination and the resulting loss of energy as heat. Holes can be trapped by water molecules or hydroxyl ions adsorbed at the catalyst surface, leading to the formation of hydroxyl radicals ($^{\bullet}$OH). Electrons can be trapped by molecular oxygen, generating the superoxide radical anion. Although photogenerated holes can attack the pollutant directly, we consider the indirect pathway (via $^{\bullet}$OH) as the dominant reaction route for the degradation of 4-CP [13,14]. In Table 2, X_i represents the organic intermediates of the reaction (i.e., 4-CC and HQ) that are further degraded by oxidation with the $^{\bullet}$OH radical, and Y_i represents inorganic radicals and species that compete with the organic substrate for the existing $^{\bullet}$OH [21].

The derivation of the reaction rate expressions for the photodegradation of 4-CP, 4-CC and HQ were based on the following assumptions:

(i) The hydroxyl radical attack is the main responsible for the degradation of 4-CP and the organic intermediate species [13,14].
(ii) Photocatalytic reactions occur at the surface of the catalyst particles among adsorbed species [17].
(iii) Dynamic equilibrium is achieved between the bulk and the adsorbed concentrations of water, oxygen, organic compounds, and inorganic species [21,22].
(iv) Molecular oxygen and organic compounds are considered to adsorb on different sites of the TiO_2 particle [20,23]. On the other hand, since adsorption sites for the organics are assumed to be the same, a competitive adsorption mechanism for 4-CP and its main intermediates is postulated.
(v) The kinetic micro steady state approximation is applied for the concentration of electrons, holes and hydroxyl radicals [20].
(vi) The rate of electron–hole generation is proportional to the local volumetric rate of photon absorption (LVRPA or e^a, Einstein $cm^{-3}\ s^{-1}$) [24].

Additional assumptions have been made to simplify the model [20,21,24]: (i) there are no mass transport limitations, (ii) oxygen concentration is constant and in excess with respect to the stoichiometric demand, and (iii) the concentration of water molecules and hydroxyl ions on the catalytic surface remains constant.

On the basis of these considerations, we derived the following reaction rate expressions:

$$r_{4\text{-CP},1}(\mathbf{x},t) = \frac{\alpha_{2,1}C_{4\text{-CP}}(t)}{1+\alpha_3 C_{4\text{-CP}}(t)+\alpha_1' C_{4\text{-CC}}(t)+\alpha_2' C_{HQ}(t)} \times \left(-1+\sqrt{1+\frac{\alpha_1}{a_v}e^a(\mathbf{x})}\right) \quad (5)$$

$$r_{4\text{-CP},2}(\mathbf{x},t) = \frac{\alpha_{2,2}C_{4\text{-CP}}(t)}{1+\alpha_3 C_{4\text{-CP}}(t)+\alpha_1' C_{4\text{-CC}}(t)+\alpha_2' C_{HQ}(t)} \times \left(-1+\sqrt{1+\frac{\alpha_1}{a_v}e^a(\mathbf{x})}\right) \quad (6)$$

$$r_{4\text{-CC}}(\mathbf{x},t) = \frac{\alpha_4 C_{4\text{-CC}}(t)}{1+\alpha_3 C_{4\text{-CP}}(t)+\alpha_1' C_{4\text{-CC}}(t)+\alpha_2' C_{HQ}(t)} \times \left(-1+\sqrt{1+\frac{\alpha_1}{a_v}e^a(\mathbf{x})}\right) \quad (7)$$

$$r_{HQ}(\mathbf{x},t) = \frac{\alpha_5 C_{HQ}(t)}{1+\alpha_3 C_{4\text{-CP}}(t)+\alpha_1' C_{4\text{-CC}}(t)+\alpha_2' C_{HQ}(t)} \times \left(-1+\sqrt{1+\frac{\alpha_1}{a_v}e^a(\mathbf{x})}\right) \quad (8)$$

where α_i and α_i' are kinetic parameters.

3.4. Radiation model

The evaluation of the radiation field inside the reactor was achieved by solving the radiative transfer equation (RTE) for the heterogeneous system. Because of the design characteristics of the experimental device (reactor dimensions and diffuse incoming radiation), the reactor can be modeled as a plane-parallel system with azimuthal symmetry. Then, a one-dimensional (x in space), one-directional (θ in the direction of radiation propagation) radiation transport model can be applied to solve the RTE [25]:

$$\mu\frac{\partial I_\lambda(x,\mu)}{\partial x}+\beta_\lambda I_\lambda(x,\mu)=\frac{\sigma_\lambda}{2}\int_{\mu'=-1}^{1} I_\lambda(x,\mu')\,p(\mu,\mu')\,\mathrm{d}\mu' \quad (9)$$

where I_λ is the spectral radiation intensity (Einstein $cm^{-2}\ s^{-1}\ sr^{-1}$); λ represents the radiation wavelength; x the axial coordinate (cm); β_λ the volumetric extinction coefficient (cm^{-1}); σ_λ the volumetric scattering coefficient (cm^{-1}); μ the direction cosine of the ray for which the RTE is written ($\mu = \cos\theta$); μ' the cosine of an arbitrary ray before scattering; and p represents the phase function for scattering. The extinction coefficient is defined as the sum of the absorption and scattering coefficients ($\beta_\lambda = \kappa_\lambda + \sigma_\lambda$).

The Henyey and Greenstein phase function ($p_{HG,\lambda}$) was adopted to model the radiation scattering of the TiO_2 particles [26]:

$$p_{HG,\lambda}(\mu_0)=\frac{1-g_\lambda^2}{(1+g_\lambda^2-2g_\lambda\mu_0)^{3/2}} \quad (10)$$

where g_λ is a free parameter called the asymmetry factor, and μ_0 represents the cosine of the angle between the direction of the incident and the scattered rays.

The values of g_λ and the specific coefficients (per catalyst mass concentration C_m) β^*_λ, σ^*_λ, and κ^*_λ, were calculated employing the method described in a previous work [27].

The optical effects of the reactor windows were taken into account to obtain the boundary conditions for Eq. (9). At $x = 0$ (Fig. 2b), radiation intensities are the result of two contributions: (i) the transmitted portion of the radiation arriving from outside of the reactor, and (ii) the reflected portion of the radiation coming from the suspension.

(i) The radiation coming from the lamps arrives in a diffuse way at the external side of the glass window. To reach the reacting space, radiation crosses two interfaces: air–glass, and glass-suspension. Because of refraction, the angular directions of the intensities entering the suspension ($I_{0,\lambda}$) are comprised between 0 and the critical angle θ_c.
(ii) The intensities coming from the reacting medium undergo multiple specular reflections at the reactor window. The global window reflection coefficient, $\Gamma_{W,\lambda}$, represents the reflected fraction of the radiation that returns to the suspension.

By applying a similar analysis at $x = L_R$, the following boundary conditions are derived:

$$I_\lambda(0,\mu) = I_{0,\lambda} + \Gamma_{W,\lambda}(-\mu)I_\lambda(0,-\mu), \quad 1 \geq \mu \geq \mu_c \tag{11a}$$

$$I_\lambda(0,\mu) = \Gamma_{W,\lambda}(-\mu)I_\lambda(0,-\mu), \quad \mu_c > \mu \geq 0 \tag{11b}$$

$$I_\lambda(L_R,-\mu) = I_{L_R,\lambda} + \Gamma_{W,\lambda}(\mu)I_\lambda(L_R,\mu), \quad 1 \geq \mu \geq \mu_c \tag{11c}$$

$$I_\lambda(L_R,-\mu) = \Gamma_{W,\lambda}(\mu)I_\lambda(L_R,\mu), \quad \mu_c > \mu \geq 0 \tag{11d}$$

where $\mu_c = \cos\theta_c$.

More details concerning the radiation model of the laboratory scale reactor can be found elsewhere [18].

The Discrete Ordinate Method [28] was applied to solve the radiation model. The solution of the RTE provides the radiation intensity at each point and each direction inside the reactor. In order to simplify the model, the radiation field is considered as independent of time (constant optical properties of the catalyst and steady radiation supply). Once the intensities were obtained, the LVRPA, involved in the reaction rate expression, was readily calculated as

$$e^a(\mathbf{x}) = 2\pi \int_\lambda \kappa_\lambda \int_{\mu=-1}^{1} I_\lambda(x,\mu)\,d\mu\,d\lambda \tag{12}$$

3.5. Experimental procedure

4-Chlorophenol (4-CP; Aldrich, >99%), 4-chlorocatechol (4-CC; Aldrich, 97%), and hydroquinone (HQ; Fluka, >99%) were employed without further purification. Reagent grade perchloric acid was used to adjust the pH of the samples. TiO_2 powder (>99% anatase, 9.6 $m^2\,g^{-1}$ specific surface area) was obtained from Aldrich Chemicals. Deionized and doubly distilled water was used to prepare all solutions.

The concentration of 4-CP and its reaction intermediates was measured by HPLC using a Waters chromatograph equipped with a LC-18 Supelcosil reversed phase column (Supelco).

In order to obtain the values of the kinetic parameters, experimental runs were performed at different levels of TiO_2 concentration: $(0.05,\ 0.1,\ 0.5,\ 1.0) \times 10^{-3}$ g cm^{-3}; incident radiation: (30%, 65%, 100%); and reactor length: (0.5, 1, 5 cm). The pH of the reacting suspensions was 2.5 and the initial 4-CP concentration in all experiments was 1.4×10^{-7} mol cm^{-3}.

3.6. Kinetic parameters estimation

A Levenberg–Marquardt optimization algorithm was applied to estimate the kinetic constants involved in Eqs. (5)–(8). The experimental concentrations of 4-CP, 4-CC and HQ, obtained from samples at different reaction times (a sample was taken from the tank every hour), were compared with simulation results. The optimization procedure renders the values of the parameters that minimize the differences between the model predictions and the experimental data. Under the operating conditions of the experiments, it was found that the terms $\alpha_3 C_{4\text{-CP}}(t)$, $\alpha'_1 C_{4\text{-CC}}(t)$, and $\alpha'_2 C_{HQ}(t)$ were much lower than 1, and thus could be neglected. Consequently, the final kinetic expressions employed for the parameters estimation were the following:

$$r_{4\text{-CP},1}(\mathbf{x},t) = \alpha_{2,1} C_{4\text{-CP}}(t)\left(-1 + \sqrt{1 + \frac{\alpha_1}{a_v} e^a(\mathbf{x})}\right) \tag{13}$$

$$r_{4\text{-CP},2}(\mathbf{x},t) = \alpha_{2,2} C_{4\text{-CP}}(t)\left(-1 + \sqrt{1 + \frac{\alpha_1}{a_v} e^a(\mathbf{x})}\right) \tag{14}$$

$$r_{4\text{-CC}}(\mathbf{x},t) = \alpha_4 C_{4\text{-CC}}(t)\left(-1 + \sqrt{1 + \frac{\alpha_1}{a_v} e^a(\mathbf{x})}\right) \tag{15}$$

$$r_{HQ}(\mathbf{x},t) = \alpha_5 C_{HQ}(t)\left(-1 + \sqrt{1 + \frac{\alpha_1}{a_v} e^a(\mathbf{x})}\right) \tag{16}$$

As can be deduced from the above equations, the degradation rates have a first order dependence with respect to the substrate concentration. The values of the five kinetic parameters, with the corresponding 95% confidence interval are $\alpha_1 = 1.09 \quad (\pm 0.07) \times 10^{11}$ s cm^2 Einstein^{-1}; $\alpha_{2,1} = 9.43\ (\pm 0.26) \times 10^{-6}$ cm s^{-1}; $\alpha_{2,2} = 2.18\ (\pm 0.46) \times 10^{-6}$ cm s^{-1}; $\alpha_4 = 1.29\ (\pm 0.08) \times 10^{-5}$ cm s^{-1}; and $\alpha_5 = 9.21\ (\pm\ 0.96) \times 10^{-6}$ cm s^{-1}.

The value of $\alpha_{2,1}$ is almost five times greater than that of $\alpha_{2,2}$. From this result we conclude that, under our experimental conditions, the degradation of 4-CP via 4-CC is favored, being 4-CC the most abundant primary intermediate. On the other hand, the kinetic parameters α_4 and α_5 are very similar. Consequently, for a given concentration of the intermediate species, the degradation rates of 4-CC and HQ are comparable.

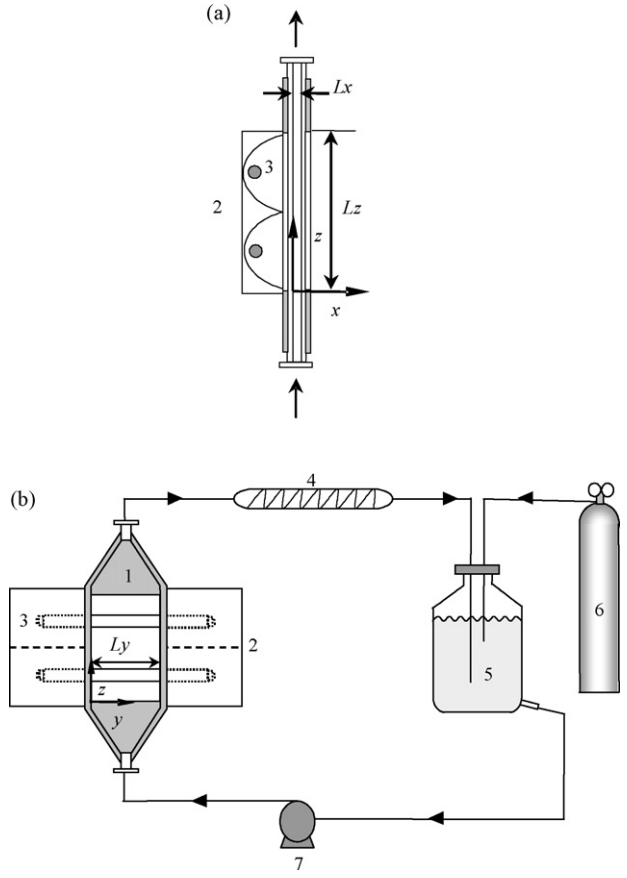

Fig. 3. Schematic representation of the bench scale experimental device. (a) Lateral view of the reactor. (b) Setup (1) front view of the reactor; (2) reflectors; (3) lamps; (4) heat exchanger; (5) tank; (6) oxygen supply; (7) pump.

4. Modeling of the bench scale reactor

4.1. Reactor description and set-up

The reactor is a thin rectangular parallelepiped that operates inside a close recycle system, as shown in Fig. 3. The reactor is limited by two parallel windows made of borosilicate glass and is illuminated from one side by two UV, tubular lamps (UV Philips TLK40/09N) placed at the focal axis of cylindrical reflectors of parabolic cross-section [29]. The recycle system has a heat exchanger to control the temperature, a storage tank with a sampling valve and an oxygen inlet, and a glass centrifugal pump. More details about the experimental device are presented in Table 1.

4.2. Mass balances

4.2.1. Mass balance in the reactor

The mass balance in the reactor is derived under the following assumptions: (i) unsteady state operation, (ii) convective laminar flow in the axial direction z ($v_x = 0$; $v_y = 0$), (iii) diffusion in the z direction is negligible with respect to convection, and (iv) symmetry in the y direction. The resulting differential equation that represents the local mass balance for a species i in the reactor, and the corresponding initial and boundary conditions are

$$\frac{\partial C_{i,\mathrm{R}}}{\partial t} + v_z \frac{\partial C_{i,\mathrm{R}}}{\partial z} - D_i \frac{\partial^2 C_{i,\mathrm{R}}}{\partial x^2} - r_i = 0, \quad i = \text{4-CP, 4-CC, HQ} \tag{17}$$

$$C_{i,\mathrm{R}}(x, z, t = 0) = C_{i,0} \tag{18}$$

$$C_{i,\mathrm{R}}(x, z = 0, t) = C^{\mathrm{o}}_{i,\mathrm{Tk}}(t) \tag{19}$$

$$\left.\frac{\partial C_{i,\mathrm{R}}}{\partial x}\right|_{x=0} = 0 \tag{20}$$

$$\left.\frac{\partial C_{i,\mathrm{R}}}{\partial x}\right|_{x=Lx} = 0 \tag{21}$$

where $C_{i,\mathrm{R}}$ denotes the molar concentration of the species i in the reactor, D_i the diffusion coefficient of i in the mixture ($\mathrm{cm^2\ s^{-1}}$), $C_{i,0}$ represents the initial concentration, and $C^{\mathrm{o}}_{i,\mathrm{Tk}}$ is the exit concentration from the tank.

The reaction rate r_i in Eq. (17), for each species considered (4-CP, 4-CC, and HQ), was replaced by the corresponding expression (Eqs. (13)–(16)) with the kinetic parameters obtained in the laboratory scale reactor.

The solution of Eqs. (17)–(21) renders the concentrations of species i as a function of x, z and t. The average exit concentration from the reactor at a given time t can be obtained from

$$\langle C_{i,\mathrm{R}}(x, z = Lz, t)\rangle_{A_R} = \frac{\int_{x=0}^{x=Lx} C_{i,\mathrm{R}}(x, z = Lz, t) v_z(x)\,\mathrm{d}x}{\int_{x=0}^{x=Lx} v_z(x)\,\mathrm{d}x} = C^{\mathrm{i}}_{i,\mathrm{Tk}}(t) \tag{22}$$

Equation (22) represents the inlet condition for the mass balance in the tank, $C^{\mathrm{i}}_{i,\mathrm{Tk}}(t)$.

4.2.2. Mass balance in the tank

Considering that the tank is perfectly stirred and operates under unsteady state conditions, the mass balance for a species i in the tank yields

$$\varepsilon_{\mathrm{L}} \left.\frac{\mathrm{d}C_i(t)}{\mathrm{d}t}\right|_{\mathrm{Tk}} = \frac{1}{\tau_{\mathrm{Tk}}}[C^{\mathrm{i}}_{i,\mathrm{Tk}}(t) - C^{\mathrm{o}}_{i,\mathrm{Tk}}(t)], \quad i = \text{4-CP, 4-CC, HQ} \tag{23}$$

with the initial condition

$$C^{\mathrm{i}}_{i,\mathrm{Tk}}(t = 0) = C_{i,0} \tag{24}$$

where τ_{Tk} is the mean residence time in the tank.

The mass balances in the reactor and tank were solved employing a finite difference numerical scheme.

4.3. Radiation model

In order to obtain the local volumetric rate of photon absorption, involved in the reaction rate expressions, the RTE was applied to the bench scale reactor. The lamps length is significantly larger than the reactor width Ly, thus uniformity of

radiation is considered along the y direction. Accordingly, a two-dimensional (x,z) model for the spatial variations of the radiation field was adopted. The angular distribution of radiation was modeled with the spherical coordinates θ and φ. The resulting form of the RTE for a two-dimensional, two-directional model is [30]

$$\mu\frac{\partial I_\lambda(x,z,\mathbf{\Omega})}{\partial x}+\eta\frac{\partial I_\lambda(x,z,\mathbf{\Omega})}{\partial z}+\beta_\lambda I_\lambda(x,z,\mathbf{\Omega}) = \frac{\sigma_\lambda}{4\pi}\int_{\mathbf{\Omega}'=4\pi} I_\lambda(x,z,\mathbf{\Omega}')\,p(\mathbf{\Omega}'\rightarrow\mathbf{\Omega})\,\mathrm{d}\mathbf{\Omega}' \quad (25)$$

where $\mu = \cos\varphi\sin\theta$ and $\eta = \sin\varphi\sin\theta$.

The boundary conditions are

$$I_\lambda(x=0,z,\mathbf{\Omega}=\mathbf{\Omega}^{\mathrm{i}}) = \chi\,(\text{properties of the emitting system and the reactor wall}) \quad (26a)$$

$$I_\lambda(x=Lx,z,\mathbf{\Omega}=\mathbf{\Omega}^{\mathrm{i}}) = \chi\,(\text{properties of the arriving radiation and the reactor wall}) \quad (26b)$$

$$I_\lambda(x,z=0,\mathbf{\Omega}=\mathbf{\Omega}^{\mathrm{i}}) = 0 \quad (26c)$$

$$I_\lambda(x,z=Lz,\mathbf{\Omega}=\mathbf{\Omega}^{\mathrm{i}}) = 0 \quad (26d)$$

where $\mathbf{\Omega}^{\mathrm{i}}$ represents the directions of radiation intensity entering the reactor.

The y–z plane represents the irradiated wall, as can be seen in Fig. 3b. The radiation flux arriving at this wall was determined by actinometric measurements. The angular distribution of the radiation entering at $x = 0$ was obtained from an emission model that takes into account the direct radiation from the two lamps and the indirect radiation from the corresponding reflectors [31]. The boundary conditions at the irradiated wall and at the opposite wall consider the effect of reflection and refraction at the air–glass and glass–liquid interfaces, as well as the slight absorption in the glass window thickness.

The model assumes that no radiation arrives from the superior and inferior reactor walls (x–y plane at $z = 0$ and $z = Lz$).

To solve the two-dimensional, two-directional model, the Discrete Ordinate Method was employed [28]. Afterward, the LVRPA was obtained according to

$$e^a(\mathbf{x}) = \int_\lambda \kappa_\lambda \int_{\mathbf{\Omega}} I_\lambda(x,z,\mathbf{\Omega})\,\mathrm{d}\mathbf{\Omega}\,\mathrm{d}\lambda \quad (27)$$

4.4. Experimental procedure

To validate the kinetic model in the bench scale reactor, experimental runs were conducted varying the catalyst concentration ($C_\mathrm{m} = 0.05,\ 0.1,\ 0.5,\ 1.0\times10^{-3}$ g cm^{-3}), and the 4-CP initial concentration ($C_{\text{4-CP},0} = 0.7$ and 1.4×10^{-7} mol cm^{-3}). The same reagents and methods of analysis described previously for the laboratory scale reactor were used in the validation procedure.

4.5. Experimental and predicted results

Fig. 4a shows the model and experimental concentrations of 4-CP, 4-CC and HQ as a function of time, for $C_\mathrm{m} = 0.5\times10^{-3}$ g cm^{-3}. It can be observed that the concentration of 4-CP decreases throughout the experimental run following a first order kinetics. After 6 h of irradiation, the pollutant has been completely degraded. The formation and destruction of the two main intermediates are also shown in the figure. The concentrations of 4-CC and HQ initially rise and reach a maximum (around the first hour for the C_m employed). Then, the intermediates species decrease slowly until they almost disappear at the end of the run. The changes in the 4-CC and HQ concentrations are in agreement with the proposed

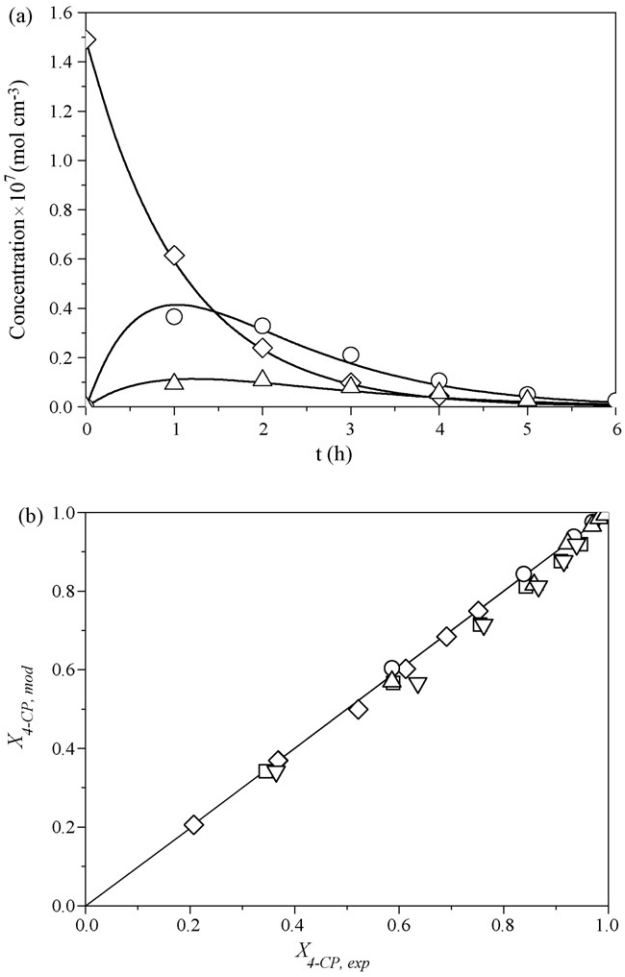

Fig. 4. (a) Experimental and predicted concentrations vs. time for $C_\mathrm{m} = 0.5\times10^{-3}$ g cm^{-3}. Solid line: model predictions. Symbols: experimental data. (◇) 4-CP, (○) 4-CC, (△) HQ. (b) Experimental vs. predicted conversions of 4-CP. Symbols correspond to different runs: (◇) $C_{\text{4-CP},0} = 1.4\times10^{-7}$ mol cm^{-3} and $C_\mathrm{m} = 0.05\times10^{-3}$ g cm^{-3}, (□) $C_{\text{4-CP},0} = 1.4\times10^{-7}$ mol cm^{-3} and $C_\mathrm{m} = 0.1\times10^{-3}$ g cm^{-3}, (○) $C_{\text{4-CP},0} = 1.4\times10^{-7}$ mol cm^{-3} and $C_\mathrm{m} = 0.5\times10^{-3}$ g cm^{-3}, (△) $C_{\text{4-CP},0} = 1.4\times10^{-7}$ mol cm^{-3} and $C_\mathrm{m} = 1.0\times10^{-3}$ g cm^{-3}, (▽) $C_{\text{4-CP},0} = 0.7\times10^{-7}$ mol cm^{-3} and $C_\mathrm{m} = 0.1\times10^{-3}$ g cm^{-3}.

kinetic mechanism of parallel formation of the two primary intermediates.

For the bench scale reactor, experimental versus predicted conversions of 4-CP are depicted in Fig. 4b. The symbols correspond to the conversion values obtained at different reaction times, for all the runs performed in this reactor. Very good agreement was found between simulation results and experimental data. The root mean square error (RMSE), based on the experimental and predicted concentrations of 4-CP and 4-CC, was 9.91%. HQ was not taken into account to compute the RMSE due to the low concentrations obtained during the experiments.

5. Conclusions

A methodology has been proposed to scale-up photocatalytic slurry reactors employing purely laboratory information, avoiding the need of using adjustable parameters for each different application of the same process. For this purpose, the 4-CP degradation has been studied in a laboratory scale reactor, obtaining kinetic expressions that involve all the significant variables that influence the reaction. These expressions are independent of the chosen reactor geometry and operation mode, and have shown to be appropriate to predict the performance of a reactor of different size, configuration and operating conditions. This is a valid indication that the proposed methodology can be very useful for applying these scale-up procedures to larger, commercial size photoreactors.

Acknowledgments

The authors are grateful to Universidad Nacional del Litoral (UNL), Consejo Nacional de Investigaciones Científicas y Técnicas (CONICET) and Agencia Nacional de Promoción Científica y Tecnológica (ANPCyT) for the financial support. They also thank Antonio C. Negro and Miguel A. Citroni for their valuable help during the experimental work.

References

[1] M.R. Hoffmann, S.T. Martin, W. Choi, D.W. Bahnemann, Chem. Rev. 95 (1995) 69.
[2] J.M. Herrmann, Catal. Today 53 (1999) 115.
[3] D. Bahnemann, Sol. Energy 77 (2004) 445.
[4] A.E. Cassano, O.M. Alfano, Catal. Today 58 (2000) 167.
[5] G. Li Puma, P.L. Yue, Chem. Eng. Sci. 58 (2003) 269.
[6] J. Giménez, D. Curcó, M.A. Queral, Catal. Today 54 (1999) 229.
[7] M.D. Labas, C.S. Zalazar, R.J. Brandi, C.A. Martín, A.E. Cassano, Helv. Chim. Acta 85 (2002) 82.
[8] G. Li Puma, Environ. Sci. Technol. 37 (2003) 5783.
[9] G. Li Puma, J.N. Khor, A. Brucato, Environ. Sci. Technol. 38 (2004) 3737.
[10] Z.J. Zhang, W.A. Anderson, M. Moo-Young, Int. J. Chem. Reactor Eng. 1 (2003) A57.
[11] Z.J. Zhang, W.A. Anderson, M. Moo-Young, Chem. Eng. Sci. 58 (2003) 911.
[12] M. Rodríguez, S. Malato, C. Pulgarin, S. Contreras, D. Curcó, J. Giménez, S. Espulgas, Sol. Energy 79 (2005) 360.
[13] A. Mills, S. Morris, R. Davies, J. Photochem. Photobiol. A 70 (1993) 183.
[14] J. Theurich, M. Lindner, D.W. Bahnemann, Langmuir 12 (1996) 6368.
[15] U. Stafford, K.A. Gray, P.V. Kamat, Res. Chem. Intermed. 23 (1997) 355.
[16] C. Minero, F. Catozzo, E. Pelizzetti, Langmuir 8 (1992) 481.
[17] E. Pelizzetti, C. Minero, Electrochim. Acta 38 (1993) 47.
[18] M.L. Satuf, R.J. Brandi, A.E. Cassano, O.M. Alfano, Ind. Eng. Chem. Res. 46 (2007) 43.
[19] M.I. Cabrera, A.C. Negro, A.E. Cassano, J. Catal. 172 (1997) 380.
[20] C.S. Turchi, D.F. Ollis, J. Catal. 122 (1990) 178.
[21] C.B. Almquist, P.A. Biswas, Chem. Eng. Sci. 56 (2001) 3421.
[22] M.F.J. Dijkstra, H.J. Panneman, J.G.M. Winkelman, J.J. Kelly, Chem. Eng. Sci. 57 (2002) 4895.
[23] R. Terzian, N. Serpone, C. Minero, E. Pelizzetti, H. Hidaka, J. Photochem. Photobiol. A 55 (1990) 243.
[24] O.M. Alfano, M.I. Cabrera, A.E. Cassano, J. Catal. 172 (1997) 370.
[25] O.M. Alfano, A.C. Negro, M.I. Cabrera, A.E. Cassano, Ind. Eng. Chem. Res. 34 (1995) 488.
[26] R. Siegel, J.R. Howell, Thermal Radiation Heat Transfer, fourth ed., Hemisphere Publishing Corp., Bristol, PA, 2002.
[27] M.L. Satuf, R.J. Brandi, A.E. Cassano, O.M. Alfano, Ind. Eng. Chem. Res. 44 (2005) 6643.
[28] J.J. Duderstadt, W.R. Martin, Transport Theory, Wiley, New York, 1979.
[29] R.J. Brandi, G. Rintoul, O.M. Alfano, A.E. Cassano, Catal. Today 76 (2002) 161.
[30] R.J. Brandi, O.M. Alfano, A.E. Cassano, Chem. Eng. Sci. 54 (1999) 2817.
[31] R.J. Brandi, O.M. Alfano, A.E. Cassano, Chem. Eng. Sci. 51 (1996) 3169.